LETTERS

Controlling cavity reflectivity with a single quantum dot

Dirk Englund[1]*, Andrei Faraon[1]*, Ilya Fushman[1]*, Nick Stoltz[2], Pierre Petroff[2] & Jelena Vučković[1]

Solid-state cavity quantum electrodynamics (QED) systems offer a robust and scalable platform for quantum optics experiments and the development of quantum information processing devices. In particular, systems based on photonic crystal nanocavities and semiconductor quantum dots have seen rapid progress. Recent experiments have allowed the observation of weak[1] and strong coupling[2,3] regimes of interaction between the photonic crystal cavity and a single quantum dot in photoluminescence. In the weak coupling regime[1], the quantum dot radiative lifetime is modified; in the strong coupling regime[3], the coupled quantum dot also modifies the cavity spectrum. Several proposals for scalable quantum information networks and quantum computation rely on direct probing of the cavity–quantum dot coupling, by means of resonant light scattering from strongly or weakly coupled quantum dots[4–9]. Such experiments have recently been performed in atomic systems[10–12] and superconducting circuit QED systems[13], but not in solid-state quantum dot–cavity QED systems. Here we present experimental evidence that this interaction can be probed in solid-state systems, and show that, as expected from theory, the quantum dot strongly modifies the cavity transmission and reflection spectra. We show that when the quantum dot is coupled to the cavity, photons that are resonant with its transition are prohibited from entering the cavity. We observe this effect as the quantum dot is tuned through the cavity and the coupling strength between them changes. At high intensity of the probe beam, we observe rapid saturation of the transmission dip. These measurements provide both a method for probing the cavity–quantum dot system and a step towards the realization of quantum devices based on coherent light scattering and large optical nonlinearities from quantum dots in photonic crystal cavities.

In the experiment, a narrow-bandwidth laser beam is scanned through the resonance of a GaAs photonic crystal cavity (Fig. 1c). The cavity contains a strongly coupled InAs quantum dot that splits its spectrum into two polariton states and causes the cavity transmission to vanish at the quantum dot frequency[14]. A linear three-hole defect in the photonic crystal forms the cavity[15] with a resonant mode at $\lambda = 926$ nm and measured quality factor $Q = 1.0 \times 10^4$ (corresponding to a cavity linewidth of $\Delta\lambda_{cav} \approx 0.10$ nm). We observe a polariton splitting of 0.05 nm. The photonic crystal was fabricated on a quantum dot wafer grown by molecular beam epitaxy, as described in Methods.

The principle of the measurement is explained in Fig. 1b. It is difficult to observe the cavity spectrum directly, because only a small fraction of the incident light couples to the photonic crystal cavity owing to poor mode matching between the gaussian probe beam and the cavity mode. For that reason, the signal reflected by the cavity is monitored in cross-polarization. This is analogous to observing transmission through a polarizing cavity inserted between two crossed polarizers. A GaAs/AlAs distributed Bragg reflector underneath the photonic crystal membrane effectively creates a single-sided cavity system and enhances the collection efficiency of the probe beam. The horizontal $|H\rangle$ component of the scattered probe beam then carries the cavity reflectivity R, as given by equation (2).

Reflectivity is measured by scanning the narrow-linewidth probe laser beam through the cavity resonance (Fig. 1a, b). In this way, we greatly exceed the 0.03 nm resolution of the spectrometer in order to sample the narrow spectral features of the system (that is, 0.05 nm Rabi splitting). To avoid difficulties related to laser stability and power normalization, we keep the laser wavelength fixed and instead scan the cavity and quantum dot using our recently developed local temperature-tuning technique[16]. The technique uses a laser beam to heat the suspended structure depicted in Fig. 1c, which is composed of a photonic crystal cavity and a heating pad. The structure was fabricated by electron beam lithography and reactive ion etching. The pad is coated with a Cr/Au metal layer to increase absorption of the 905 nm heating laser, which is tuned to this wavelength to minimize the carrier excitation in GaAs and thus reduce background photoluminescence. The sample is maintained at an average temperature of 27 K and probed using the confocal microscope set-up in Fig. 1a. The reflectivity signal from a different cavity without coupled quantum dots is shown in Fig. 1d. Here, the cavity resonance is swept through the tunable probe laser line using the local heating technique. A half-wave plate in front of the sample corrects for non-optimal orientation of the cavity and maximizes its visibility in the reflected signal (Fig. 1a). We verified that the visibility vanishes when the probe polarization is orthogonal or parallel to the cavity polarization. We obtain a cavity signal-to-background ratio of unity, which together with the imperfect extinction ratio of the polarizing beam splitter, lets us estimate that the coupling efficiency into the cavity mode is 1–2%. A more detailed explanation of how the measurement was performed is presented in Methods.

We first characterize the quantum dot–photonic crystal cavity system by photoluminescence when pumped with a continuous-wave laser beam at 780 nm, above the GaAs bandgap (incident power ~20 nW before the objective). For low excitation powers, the quantum dot photoluminescence increases linearly with pump power, indicating a single exciton line. As the quantum dot is temperature-tuned through the cavity, clear anticrossing between the quantum dot and the cavity lines is observed: the quantum dot splits the cavity spectrum into two polariton peaks (with frequencies $\omega_{\pm}$) when it becomes resonant with the cavity (Fig. 2c). This splitting is described by

$$\omega_{\pm} = \frac{\omega_c + \omega_d}{2} - i\frac{\kappa + \gamma}{2} \pm \sqrt{g^2 + \frac{1}{4}(\delta - i(\kappa - \gamma))^2} \qquad (1)$$

where ω_c denotes the cavity frequency, ω_d the quantum dot frequency, $\delta = \omega_d - \omega_c$ the quantum dot–cavity detuning, cavity field decay rate $\kappa/2\pi = 16$ GHz (linewidth 0.1 nm), Rabi frequency $g/2\pi = 8$ GHz

[1]Ginzton Laboratory, Stanford University, Stanford, California 94305, USA. [2]Department of Electrical and Computer Engineering, University of California, Santa Barbara, California 93106, USA.
*These authors contributed equally to this work.

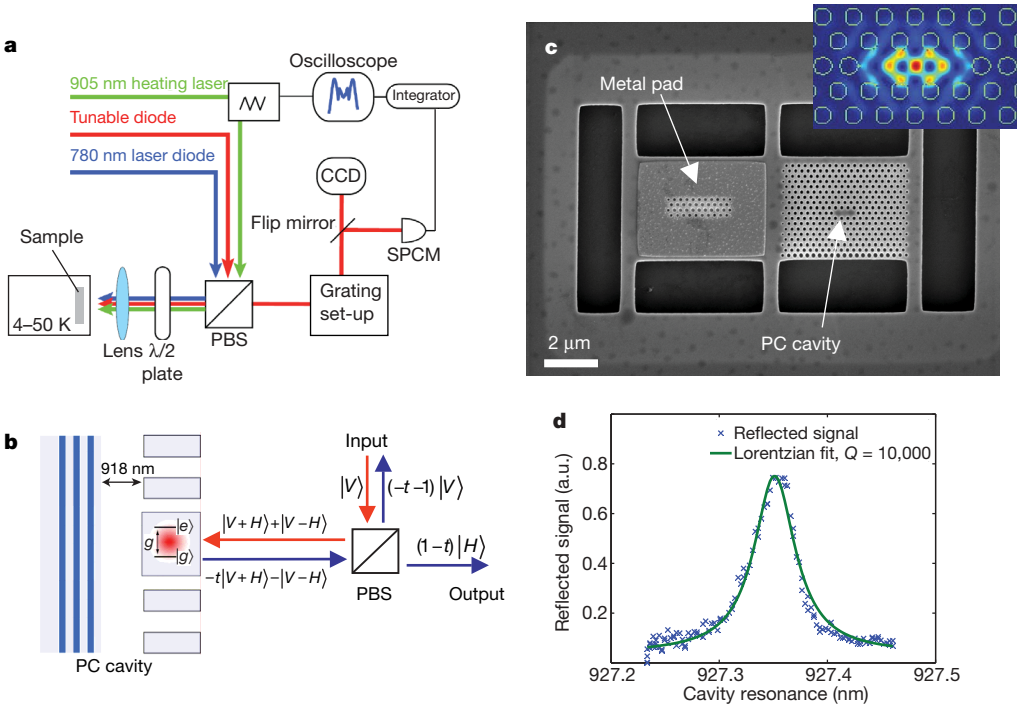

Figure 1 | Experiment set-up. a, Confocal microscope set-up. A 780 nm laser diode excites photoluminescence, while a 905 nm modulated Ti:sapphire laser locally heats the sample to tune cavity and quantum dot[16]. The reflectivity is measured with a narrow-band tunable diode laser (focal spot diameter ~1 μm for all beams). A grating set-up monitors the photoluminescence and filters the reflectivity signal from background noise. The filtered reflected signal is detected by a single photon counting module (SPCM). **b**, Principle of the reflectivity measurement off a photonic crystal (PC) cavity. A vertical ($|V\rangle$-polarized) probe laser is directed onto the linearly polarized cavity oriented at 45° ($|V+H\rangle$). Owing to interaction with the cavity, the $|V+H\rangle$ component of the probe beam is reflected with a frequency-dependent coefficient $-t(\omega)$. The $|V-H\rangle$ component reflects directly with a π phase shift. The polarizing beam splitter (PBS) passes $|H\rangle$, giving a signal that is proportional to $|1-t|^2$ on the detector (see equation (2)). **c**, Suspended structure composed of a heating pad and a photonic crystal cavity. The heating laser incident on the metal pad controls local temperature[16]. Inset, simulated electric field intensity of photonic crystal cavity. **d**, Reflectivity spectrum obtained by tuning an empty cavity (no coupled quantum dot) through the probe laser, indicating $Q = 1.0 \times 10^4$.

(from Rabi splitting of $2g$ corresponding to 0.05 nm), and the dipole decay rate without the cavity $g/2\pi \approx 0.1$ GHz. As $g \approx \kappa/2$, the cavity–quantum dot system operates at the onset of strong coupling[14], as was also the case for other quantum dot–photonic crystal cavity QED experiments done in photoluminescence[2,3].

To accurately interpret the photoluminescence and reflectivity data, we need to know the frequency of the cavity and strongly coupled quantum dot. Direct tracking of the latter is difficult because of its modified spectrum when coupled to the cavity, and because it rapidly decreases in intensity as it exits the cavity (Fig. 2b). This problem is solved by instead tracking a nearby quantum dot that precisely follows, at a fixed offset, the strongly coupled quantum dot's trajectory (Fig. 2a). Based on this, the strongly coupled quantum dot wavelength is shown in the inset of Fig. 2b, together with that of the

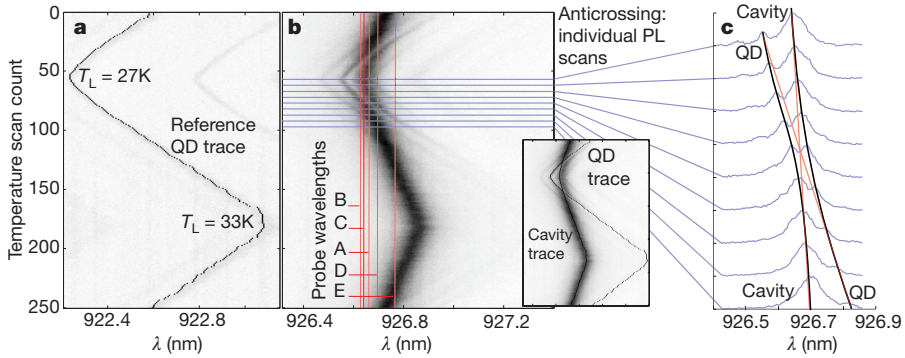

Figure 2 | Photoluminescence of a single quantum dot tuned through strong coupling to a photonic crystal cavity. The dot is excited using an above-band pump beam (780 nm wavelength, with 20 nW power incident on the sample surface). Tuning of the quantum dot through the cavity resonance is achieved following our earlier work[16], with a heating beam intensity-modulated between 6 μW and 300 μW to change local temperature T_L from 27 K to 33 K. **a**, A reference quantum dot (QD) is used for tracing the wavelength of the strongly coupled quantum dot, as dots that are closely spaced in wavelength exhibit identical temperature tuning behaviour. The heating beam power is modulated with a triangular pattern and shifts the quantum dot nearly linearly. **b**, Photoluminescence (PL) emission shows the strongly coupled quantum dot tuned in and out of resonance with a photonic crystal cavity ($Q \approx 1.0 \times 10^4$). In the reflectivity measurements, the above-band pump is switched off and the cavity/quantum dot system probed at different detunings of the reflected laser beam from the point of anticrossing (lines A–E). Inset, quantum dot and cavity traces. **c**, Individual photoluminescence cross-sections show anticrossing between quantum dot and cavity, with measured Rabi splitting of 0.05 nm (corresponding to $2g$, where the coupling strength $g/2\pi = 8$ GHz). As a guide the eye, we show the wavelengths of the uncoupled quantum dot and cavity (red line).

cavity, which shifts at a rate equal to 0.28 of the rate of the quantum dot shift.

The reflectivity of the quantum dot–cavity system is probed at five different spectral detunings $\Delta\lambda = \lambda - \lambda_0$ of the probe laser from λ_0, the anticrossing point of quantum dot and cavity (inset Fig. 3a). The incident power is in the weak excitation limit at 3 nW (measured before the objective lens), corresponding to less than one photon inside the cavity per cavity lifetime, as required for probing the vacuum Rabi splitting. For each reflectivity scan, a corresponding photoluminescence scan is obtained to track quantum dot and cavity wavelengths. Figure 3 plots the reflectivity signal as a function of temperature scan. In this data set, the temperature tuning is used to sweep the quantum dot and cavity back and forth through the probe laser. These data form the central measurement of this paper: as the single quantum dot sweeps across the cavity, it strongly modifies the reflected intensity. Instead of observing a lorentzian-shaped cavity spectrum (Fig. 1d), a drop in the reflected signal is observed at the quantum dot wavelength, as expected in the strong coupling regime. From a quantum mechanical perspective, when the quantum dot is on resonance with the cavity and strongly coupled to it, the quantum dot–cavity system does not have an energy eigenstate at the bare quantum dot resonance, and photons resonant with the quantum dot cannot be coupled into the cavity (Fig. 1b).

The reflected signal from the described cavity is derived following refs 6 and 8. The spectrum R of the reflected probe signal after the polarizing beam splitter is then given by

$$R = \eta \left| \frac{\kappa}{i(\omega_c - \omega) + \kappa + \frac{g^2}{i(\omega_d - \omega) + \gamma}} \right|^2 \qquad (2)$$

where η accounts for the efficiency of coupling to, and collecting from, the cavity. We fitted this relation to the observed spectrum, using the above-mentioned cavity–quantum dot parameters, together with the tracked quantum dot and cavity wavelengths shown at the bottom of Fig. 3a. The experimental data in the top panel of Fig. 3a show smoother features than the plot of equation (2) based on tracked quantum dot and cavity lines (dashed line). We attribute this difference to spectral fluctuations in the quantum dot and cavity that are below the resolution limit of the spectrometer, but that are greater than the linewidth of the probe beam. These fluctuations arise from instabilities in the power of the heating laser of ~0.7%. When thermal fluctuation in the quantum dot–cavity wavelength is taken into account as a gaussian broadening with full-width at half-maximum of 0.005 nm, the theoretical model matches the data (black fits).

The fits yield values for coupling strength g and cavity Q that agree with photoluminescence measurements in above-band pumping. The reflectivity data for the other probe wavelengths (Fig. 3b) capture the quantum dot at various detunings from the cavity–quantum dot intersection ranging from $-1.2g$ (-0.03 nm) to $4.5g$ (0.11 nm). The reflected probe drops towards zero precisely where the quantum dot crosses its wavelength, and the depth and shape of the drop changes with cavity detuning as predicted by theory. We note that an alternative model of an absorbing quantum dot[17] inside the cavity does not fit the reflectivity data, and predicts a cavity spectral linewidth that does not agree with the measured value. These measurements also point to one of the advantages of the solid-state cavity QED system: it is possible to capture the spatially fixed quantum dot in various states of detuning and at constant coupling to the cavity, whereas atomic systems are complicated by moving emitters.

In Fig. 4, we explore the nonlinear behaviour of another strongly coupled quantum dot–photonic crystal cavity system as a function of power P_{in} of the probe laser beam. This system shows the same coupling strength as the first, with $g/2\pi = 8$ GHz and $Q = 10^4$, and is probed here when the quantum dot is detuned by $\Delta\lambda = -0.012$ nm (corresponding to $-g/2$) from the anticrossing. P_{in} is increased from the low-excitation limit at 5 nW before the objective (corresponding to an average cavity photon number $\langle n_{cav}\rangle \approx 0.003$ in a cavity without a quantum dot) to the high-excitation regime with $P_{in} \approx 12\,\mu$W (corresponding $\langle n_{cav}\rangle \approx 7.3$). Here, $\langle n_{cav}\rangle$ is estimated as $\eta P_{in}/2\kappa\hbar\omega_c$, where $\eta \approx 1.8\%$ is the coupling efficiency into the cavity at this wavelength. Figure 4a shows the quantum-dot-induced reflectivity dip vanishing as P_{in} is increased by roughly three orders of magnitude. We modelled the saturation behaviour by a steady-state solution of the quantum master equation following ref. 18, using the above-mentioned measured system parameters. The cavity mode is represented by a number state basis truncated to $n = 100$ and driven by a coherent electric field with varying amplitude E. Figure 4a also plots the calculated normalized reflected intensity as a function of the cavity and quantum dot tuning with temperature (solid line). We see very good agreement when the solution is convolved with the gaussian filter accounting for spectral fluctuations arising from heating noise, as explained above. The full data are summarized in Fig. 4b, where we plot the reflectivity R at the quantum dot detuning $\Delta\lambda = -0.012$ nm, normalized by the reflectivity value R_0 for an empty cavity at the same wavelength as the probe laser (that is, for $g \to 0$). Our results agree with

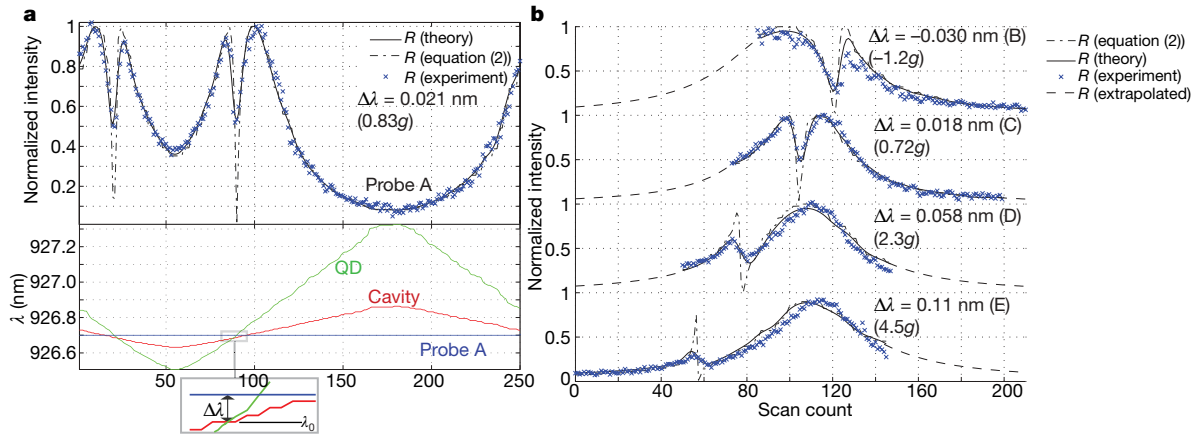

Figure 3 | Quantum dot–controlled cavity reflectivity at different probe wavelengths A–E, as indicated in Fig. 2b. a, Reflectivity spectrum of probe laser as function of quantum dot and cavity detunings, as determined from corresponding photoluminescence spectra (Fig. 2). The probe laser is detuned by $\Delta\lambda = 0.021$ nm (corresponding to $\Delta\lambda = 0.83g$) from the anticrossing point λ_0 between quantum dot and cavity (see inset). Ideal theoretical plots are calculated from equation (2). Also shown are theoretical plots that take into account a jitter (~0.005 nm) of cavity and quantum dot wavelength resulting from the heating laser power fluctuation. **b**, Probe laser at various detunings $\Delta\lambda$ from the anticrossing point samples different quantum dot–cavity detunings. Incomplete scans result from the limited range of temperature tuning.

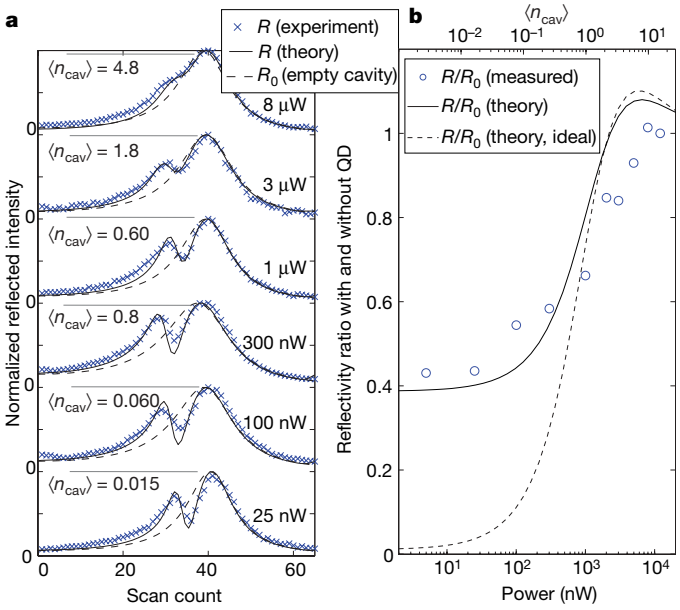

Figure 4 | Quantum-dot-controlled cavity reflectivity versus probe beam power for probe laser detuning of $\Delta\lambda = -0.012$ nm from the anticrossing point. a, Reflectivity scans at increasing probe power (measured before the objective), ranging from low-excitation to saturation regimes. The measured reflectivity is fitted by a numerical solution to the full master equation. Solutions are convolved with a gaussian filter with full-width at half-maximum of 0.005 nm to account for thermal fluctuations (solid curves). The scale for the calculated mean photon number $\langle n_{cav}\rangle$ is also indicated for each scan. Also plotted is the expected reflectivity R_0 when the quantum dot is removed (dashed curve). **b**, Reflectivity at $\Delta\lambda = -0.012$, normalized by empty-cavity reflectivity at the same wavelength, as a function of probe laser power. Saturation begins near 1 μW of input power, corresponding to $\langle n_{cav}\rangle \approx 1/2$. The dashed curve shows the reflectivity ratio if no thermal fluctuations were present. At large power, both curves tend to unity as the quantum dot–cavity spectrum approaches the lorentzian shape of the empty cavity.

the theoretical model (solid curve) and previous measurements in atomic systems[19]. Owing to the spectral fluctuations, the reflectivity does not approach zero at low power, as it would in the ideal system (dashed curve). Saturation begins at ~1 μW of incident power (measured before the objective), corresponding to $\langle n_{cav}\rangle \approx 1/2$. Taking into account the coupling efficiency η, this implies a saturation power inside the cavity of only ~20 nW, in agreement with previous predictions for giant optical nonlinearity in a microcavity[20]. We furthermore verified that the quantum-dot-induced reflectivity dip vanishes controllably when excitons are (incoherently) generated by excitation with an above-GaAs-bandgap laser beam.

In conclusion, we have experimentally demonstrated that a single quantum dot can be used to dramatically alter the reflectivity spectrum of an optical cavity. In the low-excitation regime (intracavity photon number $\langle n_{cav}\rangle \ll 1$), we observe a quantum-dot-induced change in reflectivity to 40% and find very good agreement with theory. The remaining signal is limited by measurement noise (that is, quantum dot and cavity wavelength fluctuations resulting from power instabilities of the heating laser), and should vanish with improved experimental stability. As the resonant beam intensity is increased, we observe saturation of the quantum-dot-induced dip at ~20 nW of cavity-coupled power (photon number $\langle n_{cav}\rangle \approx 1/2$), closely matched by theory. Our measurements rely on a novel quantum dot–cavity tuning and cross-polarized reflectivity method that permits resolution of ~0.005 nm (full-width at half-maximum) and high cavity–quantum dot visibility. The photonic crystal architecture is ideally suited for extending this system to greater numbers of quantum dots and cavities interconnected into a quantum network[21]. Such an on-chip approach greatly increases the coupling efficiency to and from the cavity[22], and our recent circuits should allow efficiencies exceeding 50% while ensuring a cavity $Q > 10^4$. The demonstration of quantum-dot-controlled cavity reflectivity has far-reaching implications for quantum information processing in solid-state systems, as it opens the door to high-fidelity controlled phase gates[6], single photon detection[12], coherent transfer of quantum dot state to photon state[4], and quantum repeaters using non-destructive Bell measurements with the addition of a third long-lived quantum dot level[8]. The observed giant optical nonlinearity has promising applications for generating non-classical squeezed states of light[10,23], non-destructive photon number state measurements[24], and optical signal processing.

METHODS SUMMARY

Reflectivity measurement. A cavity with coupled quantum dot showing polariton anti-crossing was first identified in photoluminescence, using above-band excitation at 780 nm. The temperature of the cryostat and the power of the heating laser were controlled so the quantum dot periodically swept through the cavity resonance. Then the tunable diode laser used for reflectivity measurements was set to the desired wavelength using the spectrometer. After spectral alignment, the 780 nm laser was turned off, and the reflectivity signal was sent to a photodetector and optimized on an oscilloscope. Once optimized, the output was switched to the spectrometer CCD and the reflectivity signal was recorded with the spectrometer taking successive spectra at 0.2-s-long integration, while the heating laser power (and subsequently quantum dot and cavity wavelength) was modulated at 10 mHz. This scanning speed is slow enough to resolve the relevant features, as seen by the number of data points sampling the quantum-dot-induced dips in Fig. 3.

Quantum dot wafer. The photonic crystal was fabricated on a quantum dot wafer grown by molecular beam epitaxy on a Si n-doped GaAs(100) substrate with a 0.1 μm buffer layer, and a 10-period distributed Bragg reflector consisting of quarter-wave AlAs/GaAs layers to improve collection efficiency into the lens[25]. The distributed Bragg reflector is separated by a 918 nm sacrificial layer of $Al_{0.8}Ga_{0.2}As$ from the 150-nm GaAs membrane that contains a central layer of self-assembled InGaAs/GaAs quantum dots. The quantum dot density varies throughout the wafer, but in this experiment, we used the low-density area with ~100 quantum dots per μm^2.

Received 5 June; accepted 4 September 2007.

1. Englund, D. *et al.* Controlling the spontaneous emission rate of single quantum dots in a two-dimensional photonic crystal. *Phys. Rev. Lett.* **95,** 013904 (2005).
2. Yoshie, T. *et al.* Vacuum Rabi splitting with a single quantum dot in a photonic crystal nanocavity. *Nature* **432,** 200–203 (2004).
3. Hennessy, K. *et al.* Quantum nature of a strongly coupled single quantum dot-cavity system. *Nature* **445,** 896–899 (2007).
4. Cirac, J. I., Zoller, P., Kimble, H. J. & Mabuchi, H. Quantum state transfer and entanglement distribution among distant nodes in a quantum network. *Phys. Rev. Lett.* **78,** 3221–3224 (1997).
5. Imamoglu, A. *et al.* Quantum information processing using quantum dot spins and cavity QED. *Phys. Rev. Lett.* **83,** 4204–4207 (1999).
6. Duan, L. M. & Kimble, H. J. Scalable photonic quantum computation through cavity-assisted interactions. *Phys. Rev. Lett.* **92,** 127902 (2004).
7. Childress, L., Taylor, J. M., Sorensen, A. S. & Lukin, M. D. Fault-tolerant quantum repeaters with minimal physical resources and implementations based on single-photon emitters. *Phys. Rev. A* **72,** 052330 (2005).
8. Waks, E. & Vučković, J. Dipole induced transparency in drop-filter cavity-waveguide systems. *Phys. Rev. Lett.* **96,** 153601 (2006).
9. Ladd, T. D., van Loock, P. K., Nemoto, K., Munro, W. J. & Yamamoto, Y. Hybrid quantum repeater based on dispersive CQED interactions between matter qubits and bright coherent light. *N. J. Phys.* **8,** 184 (2006).
10. Birnbaum, K. M. *et al.* Photon blockade in an optical cavity with one trapped atom. *Nature* **436,** 87–90 (2005).
11. Rauschenbeutel, A. *et al.* Coherent operation of a tunable quantum phase gate in cavity QED. *Phys. Rev. Lett.* **83,** 5166–5169 (1999).
12. Nogues, G. *et al.* Seeing a single photon without destroying it. *Nature* **400,** 239–242 (1999).
13. Schuster, D. I. *et al.* Resolving photon number states in a superconducting circuit. *Nature* **445,** 515–518 (2007).
14. Kimble, H. J. in *Cavity Quantum Electrodynamics* (ed. Berman, P.) 213–219 (Academic, San Diego, 1994).
15. Akahane, Y., Asano, T., Song, B.-S. & Noda, S. High-Q photonic nanocavity in a two-dimensional photonic crystal. *Nature* **425,** 944–947 (2003).
16. Faraon, A. *et al.* Local quantum dot tuning on photonic crystal chips. *Appl. Phys. Lett.* **90,** 213110 (2007).

17. Gerardot, B. D. *et al.* Contrast in transmission spectroscopy of a single quantum dot. *Appl. Phys. Lett.* **90,** 221106 (2007).
18. Tan, S. M. A computational toolbox for quantum and atomic physics. *J. Opt. B* **1,** 424–432 (1999).
19. Hood, C. J., Chapman, M. S., Lynn, T. W. & Kimble, H. J. Real-time cavity QED with single atoms. *Phys. Rev. Lett.* **80,** 4157–4160 (1998).
20. Auffeves-Garnier, A., Simon, C., Gerard, J. M. & Poizat, J.-P. Giant optical nonlinearity induced by a single two-level system interacting with a cavity in the Purcell regime. *Phys. Rev. A* **75,** 053823 (2007).
21. Englund, D., Faraon, A., Zhang, B., Yamamoto, Y. & Vučković, J. Generation and transfer of single photons on a photonic crystal chip. *Opt. Express* **15,** 5550–5558 (2007).
22. Faraon, A., Waks, E., Englund, D., Fushman, I. & Vučković, J. Efficient photonic crystal cavity-waveguide couplers. *Appl. Phys. Lett.* **90,** 073102 (2007).
23. Reiner, J. E., Smith, W. P., Orozco, L. A., Carmichael, H. J. & Rice, P. R. Time evolution and squeezing of the field amplitude in cavity QED. *J. Opt. Soc. Am. B* **18,** 1911–1921 (2001).
24. Imoto, N., Haus, H. A. & Yamamoto, Y. Quantum nondemolition measurement of the photon number via the optical Kerr effect. *Phys. Rev. A* **32,** 2287–2292 (1985).
25. Vučković, J., Englund, D., Fattal, D., Waks, E. & Yamamoto, Y. Generation and manipulation of nonclassical light using photonic crystals. *Physica E* **32,** 466–470 (2006).

Acknowledgements Financial support was provided by the ONR Young Investigator Award, the MURI Center for photonic quantum information systems (ARO/DTO Program), the Okawa Foundation Faculty Research Grant, and the CIS Seed fund. D.E. and I.F. were also supported by the NDSEG fellowship. Work was performed in part at the Stanford Nanofabrication Facility of NNIN supported by the National Science Foundation.

Author Information Reprints and permissions information is available at www.nature.com/reprints. Correspondence and requests for materials should be addressed to J.V. (jela@stanford.edu).